Ultrafast Science
A SCIENCE PARTNER JOURNAL

RESEARCH ARTICLE

Realizing Attosecond Core-Level X-ray Spectroscopy for the Investigation of Condensed Matter Systems

Adam M. Summers[1,2†], Stefano Severino[1†], Maurizio Reduzzi[1], Themistoklis P. H. Sidiropoulos[1], Daniel E. Rivas[1,3], Nicola Di Palo[1], Hung-Wei Sun[1], Ying-Hao Chien[1], Iker León[1], Bárbara Buades[1], Seth L. Cousin[1], Stephan M. Teichmann[1], Tobias Mey[4], Klaus Mann[4], Barbara Keitel[5], Elke Plönjes[5], Dmitri K. Efetov[1], Heinrich Schwoerer[6], and Jens Biegert[1,7*]

[1]ICFO - Institut de Ciencies Fotoniques, The Barcelona Institute of Science and Technology, 08860 Castelldefels, Barcelona, Spain. [2]Linac Coherent Light Source, SLAC National Accelerator Laboratory, Menlo Park, CA 94025, USA. [3]European XFEL, Holzkoppel 4, 22869 Schenefeld, Germany. [4]Institut für Nanophotonik Göttingen e.V., Hans-Adolf-Krebs-Weg 1, 37077 Göttingen, Germany. [5]Deutsches Elektronen-Synchrotron, Notkestraße 85, 22607 Hamburg, Germany. [6]Max-Planck-Institut für Struktur und Dynamik der Materie, 22761 Hamburg, Germany. [7]ICREA, Pg. Lluís Companys 23, 08010 Barcelona, Spain.

*Address correspondence to: jens.biegert@icfo.eu
†These authors contributed equally to this work.

Citation: Summers AM, Severino S, Reduzzi M, Sidiropoulos TPH, Rivas DE, Di Palo N, Sun HW, Chien YH, León I, Buades B, Cousin SL, Teichmann SM, Mey T, Mann K, Keitel B, Plönjes E, Efetov DK, Schwoerer H, Biegert J. *Ultrafast Sci.* 2023;3:Article 0004. https://doi.org/10.34133/ultrafastscience.0004

Submitted 14 August 2022
Accepted 3 November 2022
Published 31 March 2023

Unraveling the exact nature of nonequilibrium and correlated interactions is paramount for continued progress in many areas of condensed matter science. Such insight is a prerequisite to develop an engineered approach for smart materials with targeted properties designed to address standing needs such as efficient light harvesting, energy storage, or information processing. For this goal, it is critical to unravel the dynamics of the energy conversion processes between carriers in the earliest time scales of the excitation dynamics. We discuss the implementation and benefits of attosecond soft x-ray core-level spectroscopy up to photon energies of 600 eV for measurements in solid-state systems. In particular, we examine how the pairing between coherent spectral coverage and temporal resolution provides a powerful new insight into the quantum dynamic interactions that determine the macroscopic electronic and optical response. We highlight the different building blocks of the methodology and point out the important aspects for its application from condensed matter studies to materials as thin as 25 nm. Furthermore, we discuss the technological developments in the field of tabletop attosecond soft x-ray sources with time-resolved measurements at the near and extended edge simultaneously and investigate the exciting prospective of extending such technique to the study of 2-dimensional materials.

Introduction

Many open questions in solid-state science revolve around multibody physics and correlated materials [1]. The coupled charge carrier and lattice interactions give rise to emergent phenomena such as high-temperature superconductivity, the fractional quantum Hall effect, and structural and electronic phase transitions or topological properties, which provide exciting prospects to realize devices with novel functionality, e.g., in composite 2-dimensional (2D) materials [2–4]. At the same time, a fundamental insight into charge and lattice dynamics is an essential development for smart materials designed to address major-standing needs such as efficient light harvesting, energy storage, or information processing. Understanding and describing the fundamental interactions and dynamics present in these systems, particularly how they emerge, require investigating the real-time motion of charge carriers in nonequilibrium conditions [5,6] together with lattice dynamics. In particular, determining which specific orbitals contribute to the respective electronic properties necessitates the use of probing techniques capable of orbital selectivity [7–9]. X-ray absorption spectroscopy provides such unambiguous probing of individual orbitals if K and L core-level transitions are used. The development of attosecond sources with photon energies high enough to access water-window core levels [10], i.e., attosecond soft x-ray (SXR) pulses, now empowers x-ray absorption spectroscopy for

investigating electronic properties with orbital selectivity in real time.

In the SXR regime, i.e., at photon energies higher than 120 eV, spectroscopic measurements have long been performed in large-scale facilities, primarily synchrotrons or with tabletop laser–plasma sources. In the former case, the temporal resolution available for dynamic studies has been limited by tens to hundreds of picosecond duration typical of the circulating electron bunch. Experiments with subpicosecond resolution were realized with "slicing" beamlines [11] in the early 2000s, although at substantially reduced photon flux. Recently, at free-electron lasers, attosecond bursts of radiation were detected in both in the extreme ultraviolet (XUV) [12] and in the SXR [13] spectral regions. However, these bursts occur quasi-randomly, i.e., they vary in duration, absolute time delay, and spectral content. Such variations are expected to be mitigated with the development of adequate self-referenced single-shot measurement techniques. However, the problem is compounded by the difficulty to synchronize the free-electron laser SXR bursts with, e.g., a pump laser on the sub-30-fs range. These limitations, in addition to the cost and scarcity for beam time in large-scale facilities, have further motivated the development of laboratory-scale SXR sources. Following this goal, a number of approaches in providing coherent, laboratory-based x-ray sources has seen extensive research and development. These include laser-produced plasma sources [14], coherent wake field acceleration [15,16], incoherent betatron emission [15,17,18], and high-order harmonic generation (HHG). In the latter, a spectacular progress has been made in the spectral extension [19,20] of HHG sources from the XUV to the SXR photon energy regime along with the accompanied ability to provide pulses significantly shorter than a single femtosecond [21–25].

Attosecond duration pulses in the XUV at a photon energy of 90 eV were first demonstrated in 2001 [26,27]. However, the extension of attosecond technology into the SXR regime, for core-level x-ray spectroscopy, required much further research and development because of the unfavorable ponderomotive scaling laws [28–30] and phase-matching requirements of HHG [22,31]. In particular, the ability to perform attosecond experiments in the SXR water window (284 to 543 eV), named after the high transmittance of water in this region, presented an enticing goal. This region contains the elements of the building blocks of life, namely, the K-edges of C, N, and O, as well as the L-edges of a number of heavier elements. We note that SXR radiation from HHG [20] was detected as early as 1997 [32]; however, the yield of these sources was far too low for an application or for time-resolved measurements. In 2014, we demonstrated the first water-window spanning attosecond SXR source [10] together with an x-ray absorption spectrum from an organic solid at the carbon K-edge. Further work from our group [23,33,34] detailed an approach for scaling attosecond metrology [21] and technology [22] to the SXR range. Nowadays, a number of HHG sources have followed this approach capable of producing isolated subfemtosecond pulses [21,23,25,35,36]. Equally important, these pulses exhibit ultrabroad bandwidths through the entire water window [10,22,37–39], unlocking the ability to perform time-resolved x-ray spectroscopy over multiple elemental edges simultaneously [33] or to measure the near and extended absorption edge ranges in materials [40] to extract electronic and structural information simultaneously.

Core-Level X-ray Absorption Fine Structure (XAFS) Spectroscopy for Mapping Electronic Structure

In solid-state materials, atoms of various elemental species bond together to form the macroscopic material system. This bonding is governed by the valence electron orbital configuration of the respective elements and leads to a hybridization of the valence states into the overall band structure of the system. Because Coulomb forces and exchange interaction couple nuclei and charges together, lattice motion changes the electronic structure and electronic excitation changes the lattice position. This is important when considering that the valence band (VB) properties govern the response of a system to nonequilibrium conditions and, thus, the implementation into functional devices. To fully understand, the dynamic response of a system requires disentangling the multibody interaction, i.e., the involvement of various contributions to the nonequilibrium electronic properties with both elemental and orbital specificity [8,9,41]. Core-level x-ray absorption fine structure (XAFS) spectroscopy is exactly such a tool. While the valence and high-lying semi-valence states can change significantly in the formation of macroscopic systems, the inner, core-level, electron states remain deeply bound and well confined to the atomic site.

In XAFS, x-ray photons are used to excite core electrons from the bound core-level states into the unoccupied valence states or continuum. These transitions are categorized by the core level from which they occur. Absorption from the 1s orbital is labeled as K-edge, while the L_1-edge relates to the 2s level and $L_{2,3}$-edges to the 2p level. M_1, $M_{2,3}$, and $M_{4,5}$ correspond to the 3s, 3p, and 3d levels, respectively. Higher edges continue their labeling in the same fashion. Figure 1 shows a schematic representation of a prototypical x-ray absorption profile, broken into 2 regions that relate to bound–bound and bound-free transitions of the core-level electron. The first, termed x-ray absorption near-edge structure (XANES) or near-edge XAFS, corresponds to the promotion of the core electron into a dipole-accessible, nonfilled valence state. Hence, XANES probes the unoccupied density of states (DOS) [42,43]. The second region is labeled as the extended XAFS (EXAFS) region. Here, the photoelectron wave packet can experience multiple scattering events with the surrounding atoms, resulting in modulations of the absorption profile. These interference patterns contain information about the nuclear or lattice spacings. Together, the full absorption profile allows for the measurement of both the electronic properties and the geometry of the system under investigation as shown by Buades et al. [40].

The ability to extract information about the electronic nature of a system through the x-ray absorption spectrum depends on the uniqueness of the connection between the measured x-ray photons and charge carriers or, more precisely, the unique connection between x-ray absorption spectrum and the unoccupied DOS. Moreover, to study any effect, it is paramount that we probe the material in a way that the probe does not pollute the effect to be measured, i.e., measuring "x-ray" absorption through a semi-valence electron with XUV probe light will make inferring electronic dynamics from the measured absorption spectrum of photons ambiguous, and, in addition, it will alter the electronic structure. The multiple pathways that an XUV photon induces in a system lead to multiplet effects [8,42,44]. These alterations make interpretation of the x-ray

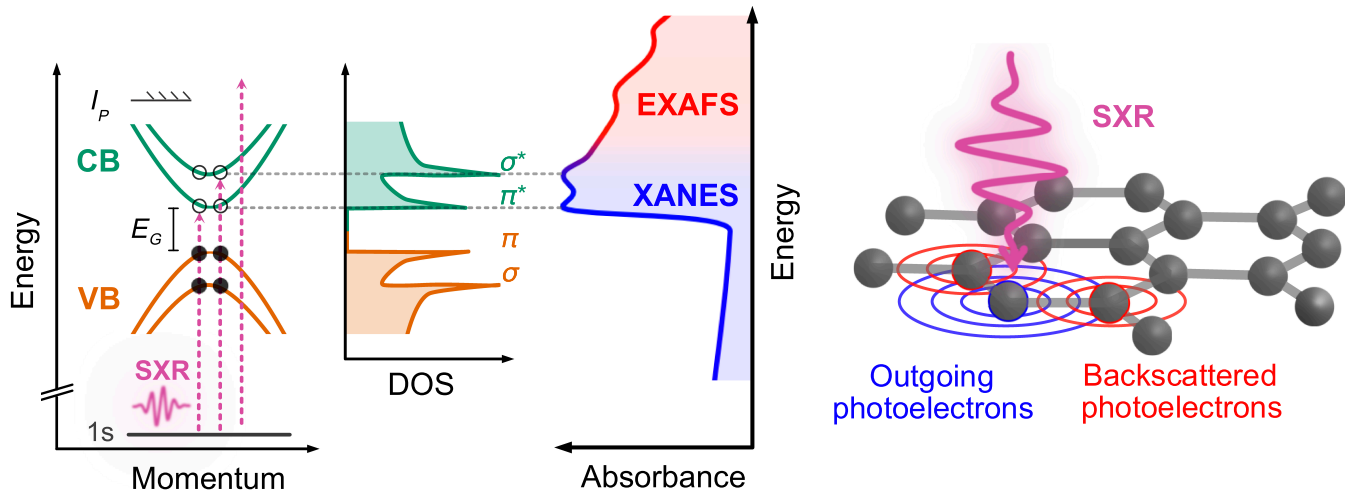

Fig. 1. Schematic representation of the x-ray absorption fine structure (XAFS) spectroscopy in a solid-state material. XAFS absorption can be understood as arising from the individual atomic contribution (in blue) and a contribution due to scattering of the photoelectron wave packet with the neighboring atoms (in red). The former, known as x-ray absorption near-edge structure (XANES), probes bound states and provide a mapping of the unoccupied density of states that are depicted along with a representative schematic of the band structure. The latter, termed extended XAFS (EXAFS), is modulated in amplitude because of the interference of the outgoing and backscattered photoelectron wave packets above the ionization potential and provides information about the spatial position of nuclei. CB, conduction band; VB, valence band; SXR, soft x-ray; DOS, density of states.

absorption spectrum, and identification of valence electronic dynamics, extremely difficult [7,8,43] without new theoretical means to disentangle these effects [8,44]. K-edge and L_1 transitions are void of such ambiguities and are thus the established transitions used in x-ray spectroscopy. We note that multiplet effects scale very poorly for higher-order transitions. For instance, probing the Ti:3d orbital of TiO_2 with XUV light from the Ti:3p (semi-valence) state generates a semi-core–hole Ti:$3p^5 3d^{N+1}$ and involves 45 pathways. Without the means to describe these pathways, the interpretation of the absorption spectrum becomes questionable. Additionally, XAFS measurements performed at low-photon energies suffer from parasitic photoionization in the higher-lying states, ($\sigma \propto Z^5 \omega^{-9/2}$), which alters the final states to be probed further [45]. Even when using x-ray photons that access K and L_1 transitions, one needs to be mindful of the core–hole effect and how it possibly alters the absorption spectrum. Here, we can draw from x-ray spectroscopy and previous measurements. In most cases, the core–hole decay is very fast or does not alter the absorption spectrum in a significant way. However, the influence of the core–hole decay, and successive Auger cascades, needs to be considered when investigating the earliest time scales until a few femtoseconds [46]. Theoretical descriptions of x-ray absorption are well established for time-stationary conditions with many powerful simulations [47–49]. The most advanced tools include multiplet effects [8], the effect of the core–hole [50–53], low-energy electron scattering [50], or phonon motion [51]. The advent of ultrafast x-ray sources nowadays challenges theory to describe transient nonlinear interactions including those effects [51,54].

Generation of SXR Pulses for Atto-XANES

As mentioned above, our progress in attosecond SXR sources has now unlocked the ability to produce isolated attosecond pulses with energies extending past 0.5 keV [21,23,33]. This has required utilizing driving laser sources in the short wavelength infrared (SWIR) spectral range (0.7 to 2.5 μm) as the maximum photon energy achievable with the HHG process scales quadratically with the driving wavelength. However, with longer driving wavelengths, the production of any appreciable SXR photon flux required the development of strategies to mitigate the unfavorable scaling of harmonic yield with wavelength (approximately scaling with λ^{-6}) [30,55,56]. A remedy was found in high-pressure phase matching [22,57], with a measured balance of ionization conditions and reabsorption. These conditions were also shown to demand a more stringent control over the carrier–envelope phase for the production of isolated attosecond SXR pulses along with acceptable spectral stability [34].

In this section, we point out several relevant results and developments implemented to reliably produce isolated SXR attosecond pulses with sufficient photon flux [10,37] to perform time-resolved x-ray [58,59] studies. We produce attosecond SXR pulses by tightly focusing a sub-2-cycle, SWIR driving laser pulse into either neon or helium. This provides a source brilliance of up to 2×10^7 photons/s/10% bandwidth at 284 eV or more than 7×10^7 photons/s on target from the carbon K-edge until the cutoff [22]. The attosecond SXR pulse is focused by a factor of 2 with an elliptical x-ray mirror (Zeiss) and detected by a homebuilt spectrograph, which consisted of a flat-field imaging grating (2,400 lines/mm; Hitachi) and a Peltier-cooled, back-illuminated charge-coupled device camera (PIXIS-XO-2048B, Princeton Instruments) with a resolution of 1/1,000, i.e., 0.3 eV at 300 eV and up to 1,500 at lower photon energies. Solid-state or gas-phase samples for transient absorption measurements are placed at the ellipsoidal focal plane. Time-resolved studies are then implemented by combining this attosecond probe pulse with an optical pump pulse in a Mach–Zehnder interferometer configuration. Furthermore, a detailed technical description of the attosecond source and experimental beamline can be found in several previous publications [10,58].

Figure 2A shows SXR spectra obtained, driving the HHG process in a high-pressure helium target with a sub-2-cycle

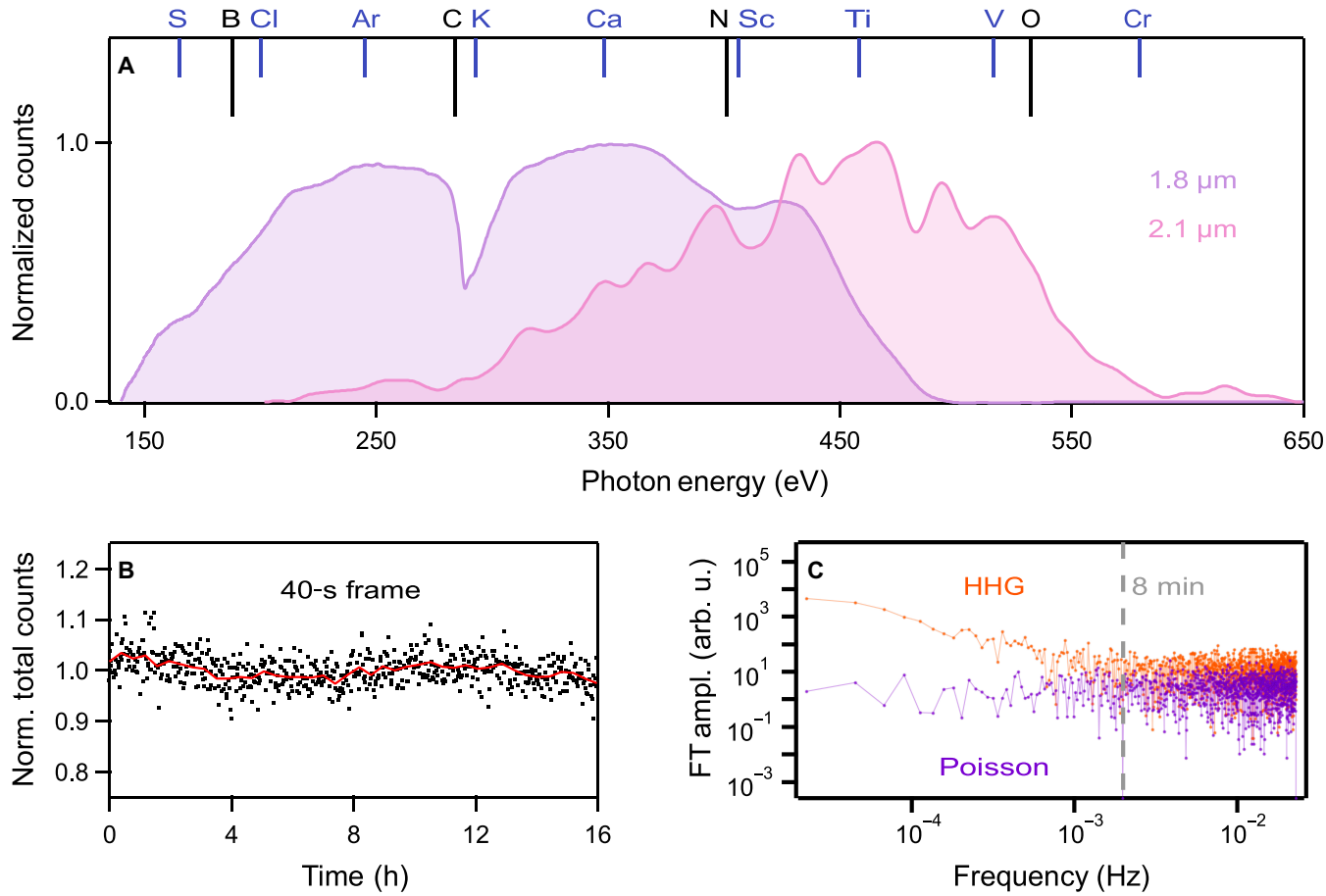

Fig. 2. Spectral and stability characterization of the ICFO Attosecond Beamline. (A) Coherent SXR continua generated with 1.85- and 2.1-μm driving pulses. Overlaid as vertical lines are the positions of accessible K (black) and L (blue) absorption edges. (B) The excellent stability of the attosecond source. The integrated number of counts per 40-s frame over 16 h fluctuates maximally by 3%. (C) Power spectrum of the integrated counts within the 1% bandwidth at the C K-edge (284 eV) (orange) compared to the one of a hypothetical shot noise limited source (violet). HHG, high-order harmonic generation; FT, Fourier transform.

1.85-μm and a 2.1-μm pulse. The bandwidth of the attosecond pulse generated using a 1.85-μm driving pulse spans the entire SXR water window and has an experimentally retrieved temporal duration of 165 as [35]. As seen from the x-ray spectrum obtained from the 2.1-μm pulse, using a longer driving wavelength allows for the production of x-ray with energies extending well past the oxygen K-edge. This extremely broad bandwidth enables x-ray absorption studies over multiple edges simultaneously (see Fig. 6). Vertical black and blue bars overlaid with the spectrum in Fig. 2A indicate the positions of principle K- and L-edges, respectively.

The exploitation of atto-XANES measurements for time-resolved applications requires high spectral stability for the entire duration of the measurement, typically on the order of several hours. To this end, Fig. 2B shows the long-term stability of the SXR attosecond beamline for 16 h where the residual fluctuations amount to 3%. This measurement clearly shows that a tabletop attosecond SXR source is perfectly capable for long-term measurements and user operation.

To more explicitly examine the noise performance for our x-ray source, we calculate the power spectrum taken over a 1% bandwidth around the carbon K-edge and compared to a simulated Poisson distribution, shown in Fig. 2C. An integration time of 40 s was used for each acquisition, and the total measurement took place over 31 h. The analysis reveals that the noise present in our source deviates strongly from the ideal white noise behavior for frequencies lower than 10^{-3} Hz, but that for higher acquisition frequencies, some overlap is achieved. This indicates that shot noise can be limited to the primary contribution to the signal-to-noise ratio (S/N). We note that it has been shown that both dark noise and readout noise can be reduced to the 10^{-3} level or below [60] in transient x-ray absorption studies, leaving photon–shot noise often the predominant contributor; see also [61].

Having discussed the stability of the source, we turn to an investigation of focusability and SXR wavefront. The high-pressure phase-matching condition, described above, to generate high-flux attosecond pulses, also has a clear effect on the wavefront of the x-ray pulse. Wavefront mismatch between pump and probe pulses in a time-resolved experiment can cause undesired effects, such as nonuniform sampling of the process under investigation and loss of temporal resolution. It is thus crucial to ensure the spatial quality of the SXR beam generated via this extremely nonlinear optical process. To investigate the spatial quality of the SXR beam and its propagation, we performed a wavefront analysis measurement utilizing a Hartmann wavefront sensor for the SXR spectral range [62,63].

In particular, the wavefront quality, divergence, and astigmatism were measured as a function of backing pressure in the HHG gas cell and with respect to the ideal conditions for maximum SXR flux generation. For this investigation, isolated attosecond pulses, with a spectrum ranging from 200 to 400 eV, were generated in neon, with a backing pressure scanned between 2 and 5 bar. Further measurements were also performed using argon as a generating medium. The Hartmann wavefront sensor is placed 20 cm after the x-ray focal plane. Figure 3A to D shows the measured wavefront at various neon backing pressures. For values between 3 and 4 bar, minimal distortion of the wavefront is observed. Consequentially, this pressure regime also corresponds to the optimum conditions for maximizing x-ray photon flux. For pressures lower than 3 bar or higher than 4 bar, the wavefront of the beam is distorted. This can be further appreciated in Fig. 3E. The measurement exhibits unequal beam aberrations as a function of the backing pressure. This is analyzed in terms of the retrieved Zernike coefficients dominated by both astigmatism coefficients that are indicative of the amount of astigmatism present. These results demonstrated that the pressure corresponding to the optimal conditions for the highest conversion efficiency is also critical in obtaining the lowest wavefront distortion and astigmatism and, thus, for a good focusing on the target for measurements. Interestingly, these measurements also show that the results are general, i.e., gas and wavelength independent. Finally, we retrieve a beam size of 15 μm at a central wavelength of 4 nm, with an M^2 value of better than 20 and an estimated root mean square of 5.7 nm.

Having discussed the spatial aspect of generation and refocusing, we now turn to the temporal synchronization. For attosecond-resolved measurements, recording temporal dynamics requires the locking (or tagging) of the phase relation between the pump pulse and the probe with subcycle resolution over the course of the entire measurement. This has remained a notoriously difficult prospect, particularly in the SXR regime where measurements typically require several hours to several days of continuous data collection. To explicitly demonstrate the capability of our beamline to track subfemtosecond dynamics, we show the results of a measurement that requires subcycle locking of pump and probe to reveal the dynamics of the autoionizing states of argon around the $L_{2,3}$-edge (see Fig. 3) [64]. In the vicinity of the $2p^{-1}$ threshold, well visible in the Ar static transmission spectrum (see Fig. 4A) are the autoionizing states 4s (244.2 eV), 5s/3d (247.0 eV), and 5s/3d (249.2 eV). Here, the sub-2-cycle, 1.85-μm pump pulse dresses the atomic system, thus dynamically changing its L-edge. Figure 4B highlights 2 of the most prominent effects of the time-resolved differential measurement: the appearance of a light-induced state at 246.0 eV and an AC Stark shift on all the 3 absorption lines, particularly on the 5s/3d state at 247.0 eV. Instantaneous temporal evolution of the pump pulse (in particular, of its electric field squared) imprinted on the AC Stark shift of the 5s/3d states is well resolved, as well as the amplitude oscillations with 3-fs periodicity (twice the frequency of the pump pulse) of the light-induced state Fig. 4C. The ability to clearly reveal the field-dressed dynamics in Ar with attosecond resolution clearly demonstrates the extremely high phase stability and phase

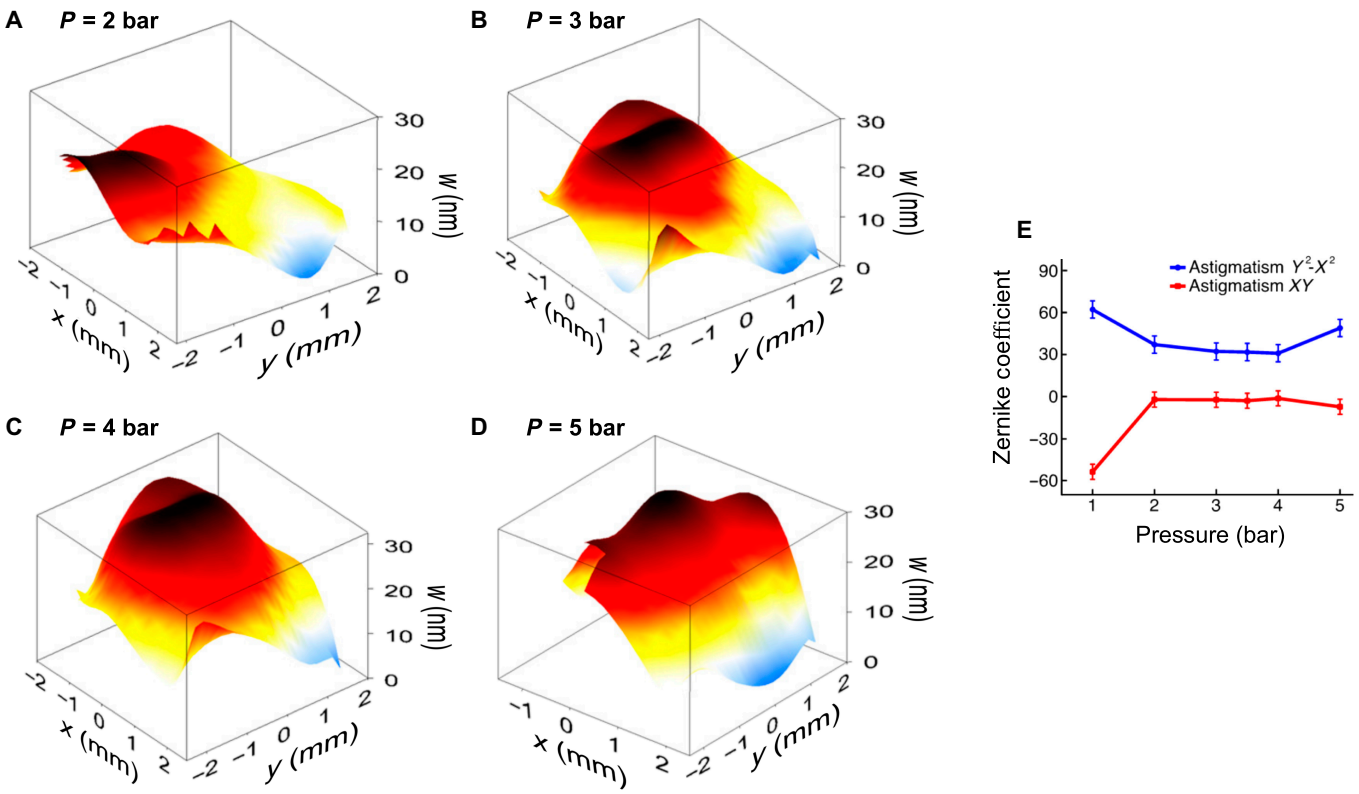

Fig. 3. Hartman wavefront measurements of the attosecond SXR wavefront for different HHG conditions. (A to D) Wavefronts and (E) the Zernike coefficients indicative of beam astigmatism. We find the lowest wavefront distortion between 3 and 4 bar, with 3.25 bar being the optimal pressure for the high-harmonics conversion efficiency. This pressure also results in lowest astigmatic aberrations (E).

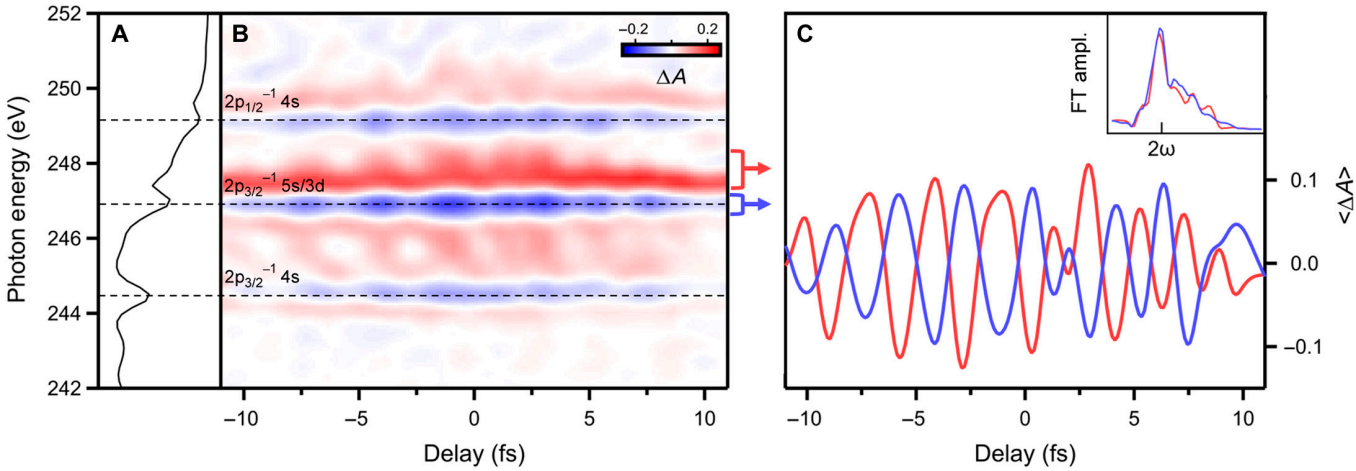

Fig. 4. Attosecond XANES $L_{2,3}$-edges in argon. (A) Time-integrated XANES of Ar shows the static transmission structure and allows to identify the relevant $L_{2,3}$ transitions (highlighted by dotted lines). (B) Attosecond time-resolved, differential absorption measurement with the 165-as SXR pulse as probe and a 1.85-μm pump pulse at a peak intensity of 10^{13} W/cm^2, resolved with a 0.5-fs step size. (C) Line-outs from (B) around the $2p_{3/2}^{-1}5s/3d$ state reveal quantum beats, and a Fourier analysis (inset) reveals a distinct contribution twice the frequency of the pump pulse.

synchronization between a sub-2-cycle pump and an attosecond SXR probe.

Electronic and Structural Information Retrieval with Atto-XANES

Atto-XANES, as described in the previous section, enables, for the first time, ultrafast time-resolved and multiedge core-level SXR absorption spectroscopy at the K- and L-edges of the elemental building blocks of highly relevant molecular and solid-state systems. In the following section, we present several results detailing the ability to use such spectroscopic measurements to extract detailed electronic and structural information.

We first like to show a comparison between the (non-time-resolved) measurement at a synchrotron light source and our attosecond beamline. We note that the majority of measurements at synchrotron facilities employ total electron yield (TEY), which measures the generated free electron current, while scanning the input x-ray energy, rather than the direct optical absorption, thus assuming that the TEY is reminiscent of the optical absorption. Figure 5 shows a comparison of 95-nm highly oriented pyrolytic graphite measured in our beamline to that of a TEY measurement performed at the Nano Magnetism Unit beamline at the ALBA Synchrotron. Graphite consists of equally oriented graphene layers, bound through Van der Waals forces, where the carbon atoms form a hexagonal lattice. The XANES structure at the carbon K-edge arises from the dipole-allowed transitions from the 1s core–shell to the unoccupied σ^* and π^* states that define the conduction band (CB) of graphite. These 2 CB states are clearly distinguishable in the x-ray absorption profiles in Fig. 5A and B. In the former, the basal plane is oriented at 40° with respect to the linearly p-polarized x-ray pulse, while in the latter is normal to the x-ray beam. As can be seen, the π^* peak at 284 eV is present for the 40° orientation while not for the 0°. This is due to the selective probing of bands with different orbital characters, here the in-plane sp_2-hybridized and the out-of-plane p_z-orbitals. A strong qualitative agreement between the results of TEY and attosecond x-ray is achieved, with the primary variation arising only from the x-ray spectrograph resolution used for each measurement. This result benchmarks our spectroscopic technique against the well-established one from large-scale facilities. Further results showing the sensitivity of atto-XANES to the various orbital contributions of graphite's DOS, as well as the retrieval of the characteristic bonding distances, can be found in [40].

A distinct advantage of K-edge spectroscopy is that the absorption is directly proportional to the unoccupied DOS. Figure 5C nicely highlights this by showing how the absorption spectrum of graphite can be easily retrieved as the product of a Fermi–Dirac distribution and the DOS, convolved with a Voigt profile to account for both the 1s core–hole lifetime broadening and spectral resolution of the x-ray spectrograph ($T_E = 350$ K and $E_F = 284.75$ eV). The DOS is obtained from density functional theory provided by the Quantum Espresso package [65]. The excellent agreement between fit and the experimental data not only proves the power of K-edge absorption spectroscopy to probe the unoccupied DOS but also opens the possibility to a reverse-fitting algorithm and retrieval of electronic temperatures and Fermi energy of an excited system as function of the delay between pump and probe.

As already mentioned, a new capability of the broad bandwidth associated with the shortness of the attosecond pulse is the possibility to perform atto-XANES measurements, simultaneously covering multiple absorption edges at the same instant in time. This can offer enormous advantages in probing the nonequilibrium electronic dynamics within the band structure of solid-state materials. Figure 6 shows the x-ray absorption spectra of hexagonal boron nitride and titanium disulfide (TiS_2), measured in the atto-XANES beamline at The Institute of Photonic Sciences.

As in the case of graphite, the lattice structure of hexagonal boron nitride consists of individual hexagonal layers bound through Van der Waals interactions, and its CB contains σ^* and π^* states. Figure 6A shows that these states are revealed in the x-ray absorption profile in both the boron K-edge, near 193 eV, and the nitrogen K-edge, near 400 eV. A peculiarity of the system is that the top of the VB (π) is primarily composed of nitrogen 2p orbitals, while the bottom of the CB (π^*) is

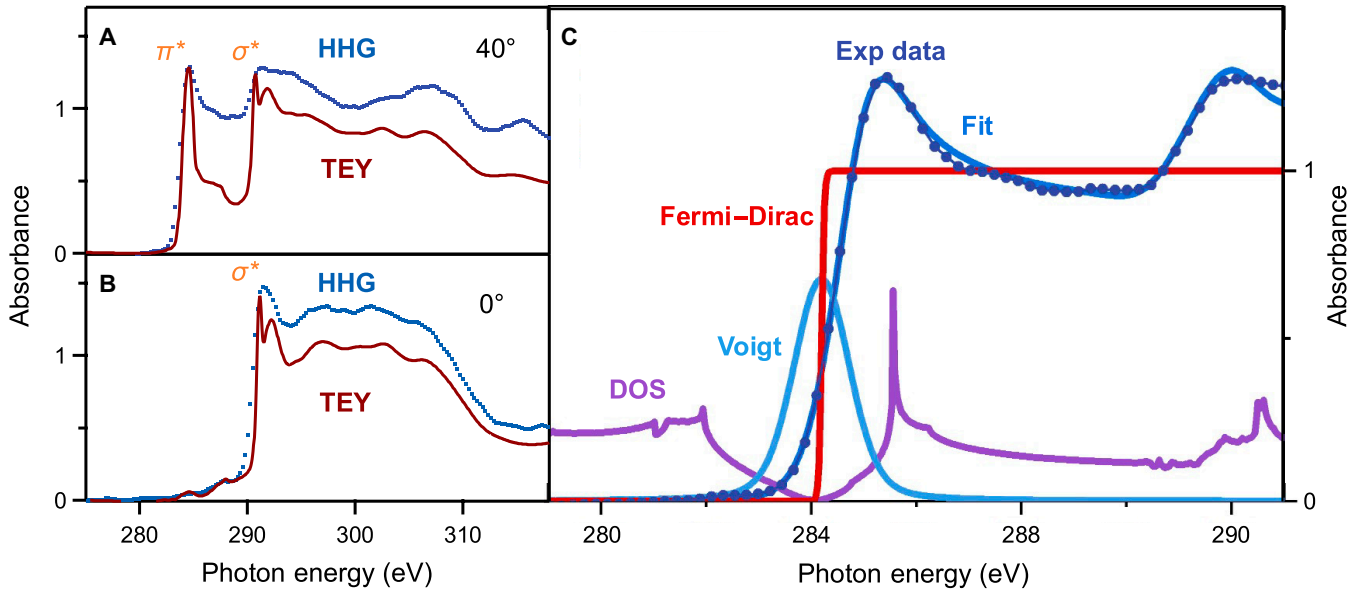

Fig. 5. Static x-ray absorption spectra from highly oriented pyrolytic graphite graphite. Benchmark comparison between the static x-ray absorption spectrum of a 95-nm-thick graphite sample measured in the Attosecond Beamline and the one of a total electron yield (TEY) measurement performed at the Nano Magnetism Unit beamline at the ALBA Synchrotron. The absorption spectrum measured both a 40° angle (A) and a 0° (B) angle of the material's basal plane with respect to the linearly polarized SXR pulse. (C) Results of the numerical fit of the XAFS spectrum of graphite described in the text, compared with the one measured in our beamline. Highlighted in different colors are the different contributions to the model.

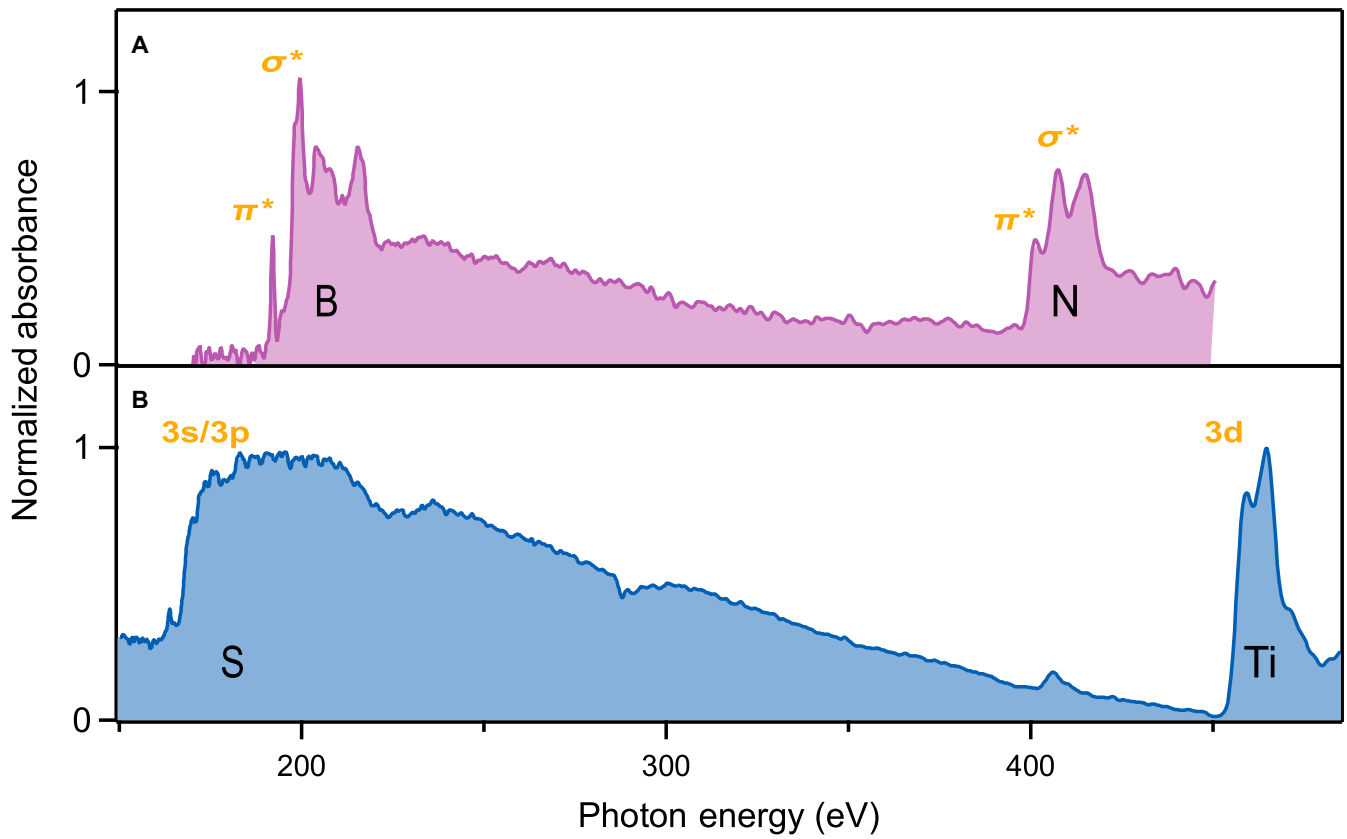

Fig. 6. X-ray absorption spectra with attosecond probe. The static x-ray absorption spectra from (A) hexagonal boron nitride and (B) titanium disulfide obtained from ultrabroad bandwidth attosecond, SXR pulses. Labeled within each panel is the state that comprises the respective absorption peaks.

primarily composed of boron 2p orbitals [66]. Hence, thanks to the ultrabroad bandwidth of the attosecond pulse, atto-XANES provides the ability to track the optical excitation from specific VBs to specific CBs in real time [66]. A further example is given in Fig. 6B by the x-ray absorption profile of the transition metal dichalcogenide TiS_2. Transition metal dichalcogenides are an exciting class of 2D materials in which correlated carrier properties could be exploited for novel optoelectronic functions or for high-density energy storage [3,5,6,67–70]. The properties of these materials nearly exclusively arise from the partially filled d-orbitals, which also exhibit strong spin–orbit coupling. Because the CB of TiS_2 has a predominantly Ti 3d character, it can be probed at the Ti $L_{2,3}$-edge at around 460 eV. The VB is instead mainly composed by mixed sulfur 3s and 3p states; thus, it can be accessed at the S $L_{2,3}$-edge at 160 eV. We have recently shown this aspect with full time-resolved atto-XANES at the Ti $L_{2,3}$-edge [58].

These examples highlight the strong benefits of SXR atto-XANES particularly well, as ultrafast correlations and electronic dynamics within the bands are simultaneously recorded. Difficulties such as repeating measurements while scanning probe photon energies and maintaining experimental conditions are inherently avoided. This is in addition to the uniquely superior temporal resolving power of atto-XANES.

The ultimate goal of the time-resolved spectroscopic technique is to track the flow of energy from the electronic photoexcitation to the relaxation of the system. Here, attosecond sources provide unique and powerful new opportunities to any existing technology. The capacity of breaking new ground with attosecond technology is evident when considering questions related to correlated multibody physics such as complex photon–carrier–phonon coupling in many relevant systems. While most conventional spectroscopic techniques do not achieve a simultaneous tracing of electron and lattice dynamics, a recent investigation by our group demonstrated that K-edge XANES meets these requirements for the first time [71].

We like to briefly point out some important aspects of the unique new attosecond capabilities with a further demonstration of atto-XANES K-edge spectroscopy. The investigation was conducted on a 25-nm-thick highly oriented pyrolytic graphite sample, which pushes signal-to-noise requirements of attosecond sources to the present limit. Less sample thickness implies a much less pronounced change in absorption, which needs to be compensated with comparatively long integration times. However, despite this difficulty, the excellent long-term stability of our attosecond source and beamline allows for such a measurement.

Specifically, we optically excite charge carriers in graphite around the K-point with an 11-fs, 1.85-μm pump pulse and track the subsequent ultrafast carrier excitation in both the CB and VB. The basal plane of the sample is oriented at 40° with respect to the linearly polarized SXR pulse to allow for the ability to probe both the π^* and the σ^* orbitals of the CB (see Fig. 5). A nonequilibrium state is induced by a delayed pump pulse with high fluence of 208 mJ/cm^2. To perform a detailed investigation of both the fast electron dynamics and subsequent phonon excitations, 2 measurements were performed: the first with a subfemtosecond resolution targeting the rising edge of the signal (first 50 fs) and the second covering the longer time dynamics of up to 10 ps. Figure 7 shows the results of this measurement over the first 500 fs. Immediately obvious are the distinct features near the Fermi energy at 284 eV in Fig. 7A. At slightly later times, an absorption increase appears around 292 eV. The aforementioned relation of x-ray absorption to unoccupied electronic states allows us then to associate these changes to the π bonding state (~284 eV) and the π^* (285 eV) and σ^* (292 eV) antibonding states. The quick rise of the π and π^* features is comparable with the pump pulse duration (see Fig. 7B). We have very recently demonstrated how to retrieve detailed information regarding the carrier–carrier scattering, enabling to disentangle between holes (π) and electrons (π^*) and to differentiate between impact excitation and Auger heating [71]. Strong electron–phonon coupling gives then rise to the delayed σ^* signal that allows to access both the incoherent and coherent phonon excitations. Its rise can be modeled with a 3-temperature rate equation model, while its oscillatory patterns allow to discern between the coherently excited phonon modes. Overall, the capacity of K-shell atto-XANES shows that the direct mapping of the DOS via the absorption constitutes an ideal probe to investigate dissipation pathways from the attosecond to the picosecond time scales, from carrier to lattice dynamics.

Aside from the rapid dynamics previously dicussed in the near-edge absorption regime, we simultaensouly observed the far-edge region EXAFS. Changes in the EXAFS due to lattice motion occur at much later delays; hence, we show in Fig. 7C a delay scan up to 25 ps at delay steps greater than 5 ps. For a simple impression where to expect changes in the EXAFS, we resort to simulations with FDMNES [72]. Figure 7D displays changes in the EXAFS for interlayer separation along the basal plane and indicates, among more complicated lattice dynamics, contributions to the measured EXAFS signal. This first time resolved EXAFS measurement demonstates the ability to use the extremely high bandwidth from isolated attosecond pulses to perform time-resolved, near, and extended-edge x-ray absorption spectroscopy.

Extending K-edge Atto-XANES to Thin Samples and Novel 2D Materials

Several rapidly advancing research directions in solid-state physics are related to the understanding of strongly correlated 2D materials. In view of exploring quantum confinement effects and correlated electron dynamics on the attosecond time scale, the enticing prospect exists to apply atto-XANES to thin or few-layer samples. The general requirement of any absorption-based techniques is finding a balance between achieving sufficient absorption to extract a signal while keeping absorption minimal to avoid lowering S/N in and self-absorption effects. A good rule of thumb in XAFS is keeping the sample thickness such that approximately 1/e of the incoming signal is transmitted to best optimize the S/N in the absorption measurement. For example, at the carbon K-edge near 284 eV, this requires a ~100-nm-thick graphite sample. In the preceding section, we detailed the successful use of a sample with a thickness much less than the x-ray absorption length in an atto-XANES measurement. These investigations showcase the feasibility of atto-XANES to investigate systems already with only a few tens of layers. The exciting and rapid current development of ultrafast laser technology, novel phase matching schemes, improved x-ray optics, and low-noise x-ray photon detectors provide very exciting prospects to extend atto-XANES measurements into 2D materials. In the following, we point out some aspects of these developments.

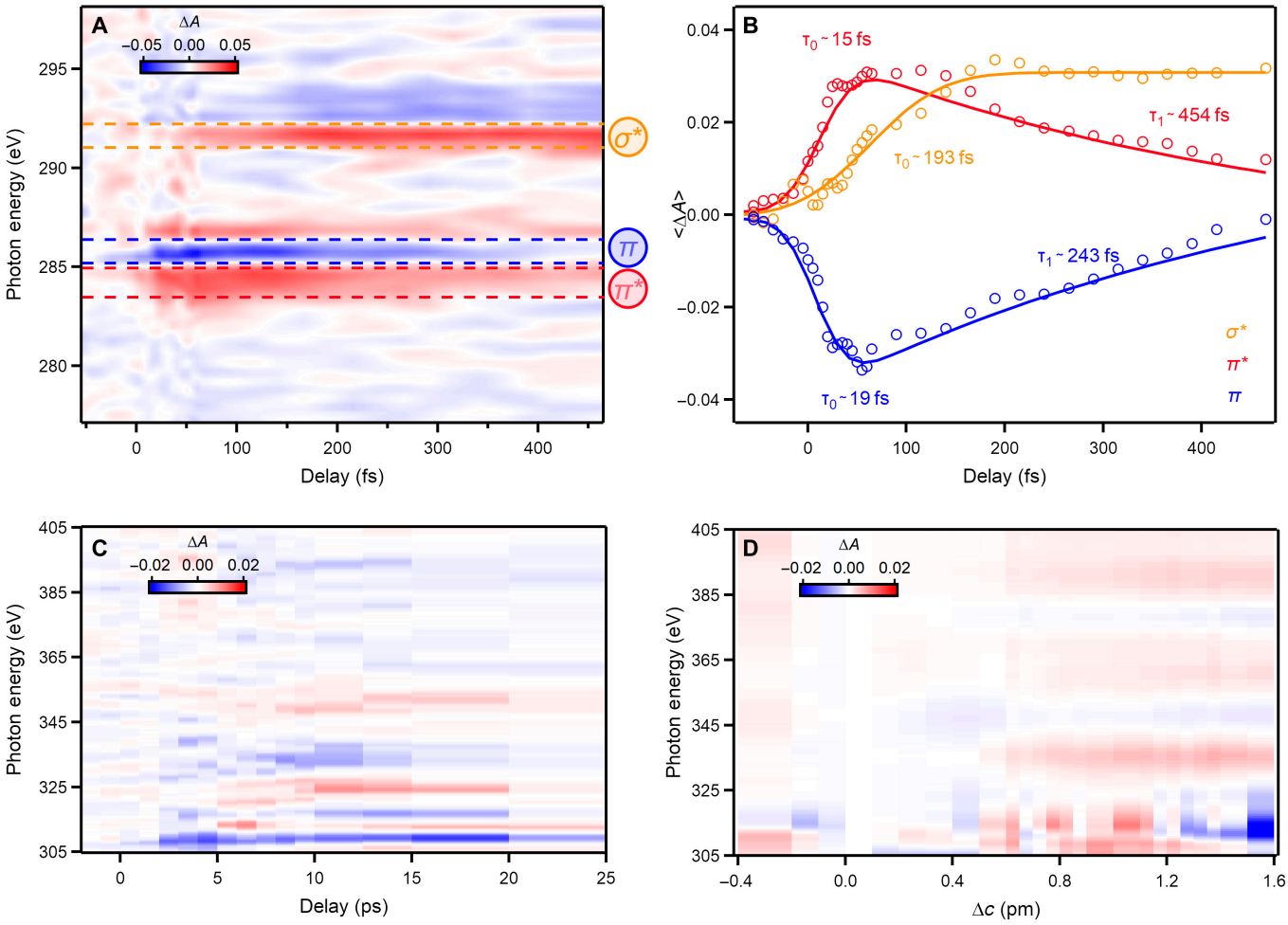

Fig. 7. Time-resolved atto-XAFS measurement in graphite. (A) The differential absorption $\Delta A(E)$ between the XANES spectrum with and without pump pulse on a 25-nm-thick graphite sample. The dynamics are photoinduced with a pump fluence of 208 mJ/cm^2 at the wavelength of 1.85 μm and probed with isolated attosecond pulses at the C K-edge (284.5eV). (B) Average of ΔA over the respective energy range for π^*(blue), π^* (red), and σ^* (orange) fit with an error function (solid lines). (C) Time-resolved EXAFS region of the same sample, shown for a long-range delay scan to 25 ps. (D) FDMNES simulation of expected changes in the EXAFS for interlayer separation out of equilibrium.

In addition to generating a comparatively high photon flux from HHG-based sources, a known challenge for the manipulation of x-ray pulses is the low efficiency of optical elements due to the low refractive index contrast in the x-ray wavelength range. However, a number of exciting technological advancements in both source development and much higher efficiency x-ray optics have been recently demonstrated. On one side, active development of next-generation, ultrafast laser sources for driving the HHG process is underway. One hundred-watt-scale OPCPAs in the SWIR have become commercially available in the last few years with expected scaling to the 1-kW level [73–75]. Perhaps even more importantly, the developments of reflection zone plate-based x-ray spectrometers offer a dramatic increase in efficiency over current reflection gratings [76]. Additionally, research in better HHG phase-matching schemes offers promising further increases in the total x-ray flux [77,78]. Using specifications that we deem realistic in the near future, we perform an estimation of the signal to noise achievable in transient x-ray absorption measurements on the example of graphite.

Considering shot noise as the sole source of noise (see Fig. 2), the total noise present in a transient absorption measurement (Δ) is given by:

$$\Delta = \frac{N_0^D - N_{pp}^D}{\sqrt{N_0^D - N_{pp}^D}} \quad (1)$$

where, N_0^D and N_{pp}^D are the number of detected photons in the unpumped case and pumped case, respectively. Propagating this uncertainty for absorption measurements using the Beer–Lambert law gives the number of minimum photons ($N_0^{\min}$) produced by an x-ray source to achieve a desired S/N (β) as:

$$N_0^{\min} = \beta^2 \, \eta \, e^{\alpha_0 d} \frac{1 + e^{-\alpha_0 \sigma d}}{\left(1 - e^{-\alpha_0 \sigma d}\right)} \quad (2)$$

where η is total efficiency of the x-ray photon detection (considering losses from x-ray optics and x-ray detector efficiency), α_0 is the x-ray absorption length, σ is the relative modification of the absorption constant by the pump pulse, and d is the sample thickness.

Figure 8 shows the signal-to-noise level versus acquisition time for 4 sample thicknesses. This is calculated using a conservative input photon flux of 10^7 photons/s over 1% bandwidth and $\eta = 5.0\%$. The absorption length of graphite is 95 nm at 284 eV, and $\sigma = 0.25$ is set to match the observed change in

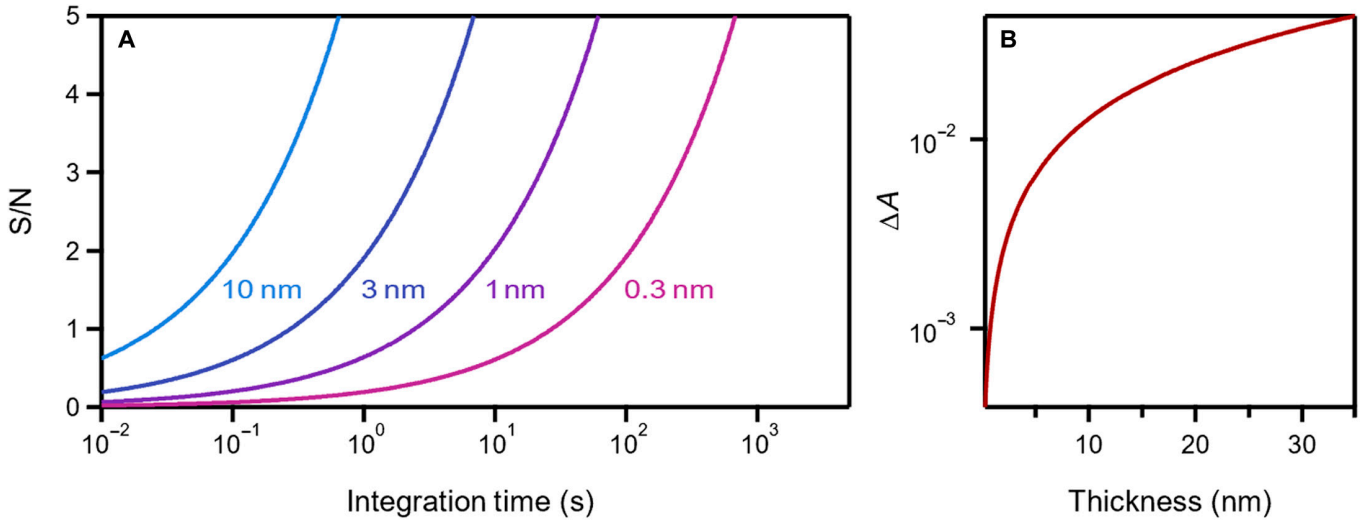

Fig. 8. Signal-to-noise estimation for few layers of samples as a function of the integration time. (A) Estimated values for different samples thicknesses, according to the model described in the text. The data shown here consider photon flux of 10^7 photons/s over 1% bandwidth. (B) The estimated differential absorption signal as function of the sample thickness used to obtain the data in (A).

absorption for the results shown in Fig 8 and [71]. As can be seen, performing atto-XANES measurements, with realistic acquisition times and S/N, on samples with thicknesses down to the few or single nanometer is possible. Note that the bulk x-ray absorption constant was used in this calculation. While the x-ray absorption in graphene has been demonstrated to scale linearly with the number of layers over a significant range of thicknesses [79], it is unclear whether the scaled bulk absorption to a single layer do not significantly underestimate the absorption of a monolayer. Additionally, when approaching this limit, one cannot neglect detector dark noise due to the increasingly small change in absorption signal level. For further consideration of the ability to resolve transient absorption features, the change in absorption induced by the pump as a function of sample thickness is shown in the inset of Fig. 8. Overall, we find that the prospects of leveraging the power of attosecond XANES for investigations of the plethora of interesting physics of 2D materials extremely exciting and promising.

Conclusion

The extension of attosecond light sources into the SXR regime provides a truly unique experimental capability for investigating ultrafast dynamics in solid-state materials. The ability to perform true XANES measurements at the K- and L-edges of a host of highly relevant elements with attosecond temporal resolution allows for the unambiguous extraction of detailed electronic structure and charge carrier populations both during optical excitation and during the subsequent dephasing processes and the relaxation into the lattice degrees of freedom. Perhaps even more important than the real-time temporal capability of atto-XANES is the capacity of the short attosecond pulse's broad coherent bandwidth to probe extensive areas around and after an edge or even across multiple edges simultaneously. The true information content of the full Wigner distribution of such a measurement has not been exploited yet. Furthermore, we expect that the technical developments on both laser front end and detection will make it feasible to apply the methodology to 2D material systems as well. Some of our demonstrations show the aforementioned prospects already. Atto-XANES and EXAFS provide powerful new tools for the real-time investigation of correlated multibody physics to address canonical questions such as superconductivity and Mott physics and, with direct application to material science, light harvesting or hydrogen fuel cells and energy storage.

Acknowledgements

Funding: J.B. acknowledges financial support from the European Research Council for ERC Advanced Grant "TRANSFORMER" (788218), ERC Proof of Concept Grant "miniX" (840010), FET-OPEN "PETACom" (829153), FET-OPEN "OPTOlogic" (899794), FET-OPEN "TwistedNano" (101046424), Laserlab-Europe (871124), Marie Skłodowska-Curie ITN "smart-X" (860553), MINECO for Plan Nacional PID2020–112664 GB-I00, AGAUR for 2017 SGR 1639, MINECO for "Severo Ochoa" (CEX2019-000910-S), Fundació Cellex Barcelona, the CERCA Programme/Generalitat de Catalunya, and the Alexander von Humboldt Foundation for the Friedrich Wilhelm Bessel Prize. S.S. acknowledges Marie Skłodowska-Curie grant agreement no. 713729 (COFUND). M.R. and A.M.S. acknowledge Marie Skłodowska-Curie Grant agreement no. 754510 (PROBIST).
Competing interests: The authors declare that there is no conflict of interest regarding the publication of this article.

Data Availability

Data is available on request.

References

1. Adler R, Kang C-J, Yee C-H, Kotliar G. Correlated materials design: Prospects and challenges. *Rep Prog Phys*. 2019;82:012504.
2. Schaibley JR, Yu H, Clark G, Rivera P, Ross JS, Seyler KL, Yao W, Xu X. Valleytronics in 2D materials. *Nat Rev Mater*. 2016;1:16055.
3. Ahmed S, Yi J. Two-dimensional transition metal dichalcogenides and their charge carrier Mobilities in field-effect transistors. *Nanomicro Lett*. 2017;9:50.

4. Keimer B, Moore JE. The physics of quantum materials. *Nat Phys*. 2017;13:1045–1055.
5. Powell JR. The quantum limit to Moore's law. *Proc IEEE*. 2008;96:1247–1248.
6. Markov IL. Limits on fundamental limits to computation. *Nature*. 2014;512:147–154.
7. Stöhr J. *NEXAFS Spectroscopy*. Heidelberg (Germany): Springer Berlin; 1992. Vol. 25.
8. de Groot F, Kotani A, *Core level spectroscopy of solids*. Boca Raton (FL): CRC Press; 2008.
9. Bunker G, *Introduction to XAFS: A practical guide to x-ray absorption fine structure spectroscopy*. Cambridge (UK): Cambridge University Press; 2010.
10. Cousin SL, Silva F, Teichmann S, Hemmer M, Buades B, Biegert J. High-flux table-top soft x-ray source driven by sub-2-cycle, CEP stable, 1.85-μm 1-kHz pulses for carbon K-edge spectroscopy. *Opt Lett*. 2014;39:5383–5386.
11. Schoenlein RW, Chattopadhyay S, Chong HHW, Glover TE, Heimann PA, Shank CV, Zholents AA, Zolotorev MS. Generation of femtosecond pulses of synchrotron radiation. *Science*. 2000;287:2237–2240.
12. Maroju PK, Grazioli C, Di Fraia M, Moioli M, Ertel D, Ahmadi H, Plekan O, Finetti P, Allaria E, Giannessi L, et al. Attosecond pulse shaping using a seeded free-electron laser. *Nature*. 2020;578:386–391.
13. Duris J, Li S, Driver T, Champenois EG, MacArthur JP, Lutman AA, Zhang Z, Rosenberger P, Aldrich JW, Coffee R, et al. Tunable isolated attosecond X-ray pulses with gigawatt peak power from a free-electron laser. *Nat Photonics*. 2020;14:30–36.
14. Mantouvalou I, Witte K, Martyanov W, Jonas A, Grötzsch D, Streeck C, Löchel H, Rudolph I, Erko A, Stiel H, et al. Single shot near edge x-ray absorption fine structure spectroscopy in the laboratory. *Appl Phys Lett*. 2016;108:201106.
15. Hussein AE, Senabulya N, Ma Y, Streeter MJV, Kettle B, Dann SJD, Albert F, Bourgeois N, Cipiccia S, Cole JM, et al. Laser-wakefield accelerators for high-resolution X-ray imaging of complex microstructures. *Sci Rep*. 2019;9:3249.
16. Hollinger R, Bargsten C, Shlyaptsev VN, Kaymak V, Pukhov A, Capeluto MG, Wang S, Rockwood A, Wang Y, Townsend A, et al. Efficient picosecond x-ray pulse generation from plasmas in the radiation dominated regime. *Optica*. 2017;4:1344–1349.
17. Behm K, Hussein AE, Zhao TZ, Baggott RA, Cole JM, Hill E, Krushelnick K, Maksimchuk A, Nees J, Rose SJ, et al. Demonstration of femtosecond broadband X-rays from laser wakefield acceleration as a source for pump-probe X-ray absorption studies. *High Energy Density Phys*. 2020;35:100729.
18. Schnell M, Sävert A, Landgraf B, Reuter M, Nicolai M, Jäckel O, Peth C, Thiele T, Jansen O, Pukhov A, et al. Deducing the electron-beam diameter in a laser-plasma accelerator using x-ray betatron radiation. *Phys Rev Lett*. 2012;108:075001.
19. Seres J, Seres E, Verhoef AJ, Tempea G, Streli C, Wobrauschek P, Yakovlev V, Scrinzi A, Spielmann C, Krausz F. Source of coherent kiloelectronvolt X-rays. *Nature*. 2005;433:596.
20. Popmintchev T, Chen M-C, Popmintchev D, Arpin P, Brown S, Ališauskas S, Andriukaitis G, Balčiunas T, Mücke OD, Pugzlys A, et al. Bright coherent ultrahigh harmonics in the keV x-ray regime from mid-infrared femtosecond lasers. *Science*. 2012;336:1287–1291.
21. Cousin SL, Di Palo N, Buades B, Teichmann SM, Reduzzi M, Devetta M, Kheifets A, Sansone G, Biegert J, Di Palo N, et al. Attosecond streaking in the water window: A new regime of attosecond pulse characterization. *Phys Rev X*. 2017;7:041030.
22. Teichmann SM, Silva F, Cousin SL, Hemmer M, Biegert J. 0.5-keV soft X-ray attosecond continua. *Nat Commun*. 2016;7:11493.
23. Silva F, Teichmann SM, Cousin SL, Hemmer M, Biegert J. Spatiotemporal isolation of attosecond soft X-ray pulses in the water window. *Nat Commun*. 2015;6:6611.
24. Chini M, Zhao K, Chang Z. The generation, characterization and applications of broadband isolated attosecond pulses. *Nat Photonics*. 2014;8:178–186.
25. Gaumnitz T, Jain A, Pertot Y, Huppert M, Jordan I, Ardana-Lamas F, Wörner HJ. Streaking of 43-attosecond soft-X-ray pulses generated by a passively CEP-stable mid-infrared driver. *Opt Express*. 2017;25:27506–27518.
26. Paul PM, Toma ES, Breger P, Mullot G, Auge F. Observation of a train of attosecond pulses from high harmonic generation. *Science*. 2001;292:1689–1692.
27. Hentschel M, Kienberger R, Spielmann C, Reider GA, Milosevic N, Brabec T, Corkum P, Heinzmann U, Drescher M, Krausz F. Attosecond metrology. *Nature*. 2001;414(6863):509–513.
28. Gordon A, Kärtner FX. Scaling of keV HHG photon yield with drive wavelength. *Opt Express*. 2005;13:2941–2947.
29. Yakovlev VS, Ivanov M, Krausz F. Enhanced phase-matching for generation of soft X-ray harmonics and attosecond pulses in atomic gases. *Opt Express*. 2007;15:15351–15364.
30. Austin DR, Biegert J. Strong-field approximation for the wavelength scaling of high-harmonic generation. *Phys Rev A*. 2012;86:023813.
31. Popmintchev T, Chen M-C, Bahabad A, Gerrity M, Sidorenko P, Cohen O, Christov IP, Murnane MM, Kapteyn HC. Phase matching of high harmonic generation in the soft and hard X-ray regions of the spectrum. *Proc Natl Acad Sci USA*. 2009;106:10516–10521.
32. Spielmann C, Burnett NH, Sartania S, Koppitsch R, Schnürer M, Kan C, Lenzner M, Wobrauschek P, Krausz F. Generation of coherent X-rays in the water window using 5-femtosecond laser pulses. *Science*. 1997;278:661–664.
33. Teichmann SM. Ponderomotively scaled high harmonic generation for attoscience in the water window [thesis]. [Barcelona (Spain)]: Universitat Politècnica de Catalunya; 2015.
34. Teichmann SM, Silva F, Cousin SL, Biegert J. Importance of intensity-to-phase coupling for water-window high-order-harmonic generation with few-cycle pulses. *Phys Rev A*. 2015;91:063817.
35. Zhao X, Wang S-J, Yu W-W, Wei H, Wei C, Wang B, Chen J, Lin CD. Metrology of time-domain soft X-ray attosecond pulses and reevaluation of pulse durations of three recent experiments. *Phys Rev Appl*. 2020;13:034043.
36. Li J, Ren X, Yin Y, Zhao K, Chew A, Cheng Y, Cunningham E, Wang Y, Hu S, Wu Y, et al. 53-attosecond X-ray pulses reach the carbon K-edge. *Nat Commun*. 2017;8:186.
37. Johnson AS, Austin DR, Wood DA, Brahms C, Gregory A, Holzner KB, Jarosch S, Larsen EW, Parker S, Strüber CS, et al. High-flux soft x-ray harmonic generation from ionization-shaped few-cycle laser pulses. *Sci Adv*. 2018;4(5):eaar3761.
38. Popmintchev D, Galloway BR, Chen MC, Dollar F, Mancuso CA, Hankla A, Miaja-Avila L, O'Neil G, Shaw JM, Fan G, et al. Near- and extended-edge X-ray-absorption fine-structure spectroscopy using ultrafast coherent high-order harmonic supercontinua. *Phys Rev Lett*. 2018;120:Article 093002.
39. Schmidt C, Pertot Y, Balciunas T, Zinchenko K, Matthews M, Wörner HJ, Wolf J-P. High-order harmonic source spanning up to the oxygen K-edge based on filamentation pulse compression. *Opt Express*. 2018;26:11834–11842.

40. Buades B, Moonshiram D, Sidiropoulos TPH, León I, Schmidt P, Pi I, Di Palo N, Cousin SL, Picón A, Koppens F, et al. Dispersive soft x-ray absorption fine-structure spectroscopy in graphite with an attosecond pulse. *Optica*. 2018;5(5):502–506.
41. Reshak AH, Kityk IV, Auluck S. Electronic structure and optical properties of 1T-TiS2 and lithium intercalated 1T-TiS2 for lithium batteries. *J Chem Phys*. 2008;129:Article 074706.
42. de Groot F. Multiplet effects in X-ray spectroscopy. *Coord Chem Rev*. 2005;249:31–63.
43. Milne CJ, Penfold TJ, Chergui M. Recent experimental and theoretical developments in time-resolved X-ray spectroscopies. *Coord Chem Rev*. 2014;277–278:44–68.
44. Roemelt M, Maganas D, DeBeer S, Neese F. A combined DFT and restricted open-shell configuration interaction method including spin-orbit coupling: Application to transition metal L-edge X-ray absorption spectroscopy. *J Chem Phys*. 2013;138:Article 204101.
45. Starace AF. Photoionization of atoms. In: Drake G, editor. *Springer handbook of atomic, molecular, and optical physics*. New York (NY): Springer New York; 2006. p. 379–390.
46. Moulet A, Bertrand JB, Klostermann T, Guggenmos A, Karpowicz N, Goulielmakis E. Soft x-ray excitonics. *Science*. 2017;357:1134–1138.
47. Newville M. EXAFS analysis using FEFF and FEFFIT. *J Synchrotron Radiat*. 2001;8:96–100.
48. Newville M. Fundamentals of XAFS. *Rev Mineral Geochem*. 2014;78:33–74.
49. Rehr JJ, Mustre de Leon J, Zabinsky SI, Albers RC. Theoretical x-ray absorption fine structure standards. *J Am Chem Soc*. 1991;113:5135–5140.
50. Joly Y. X-ray absorption near-edge structure calculations beyond the muffin-tin approximation. *Phys Rev B*. 2001;63:125120.
51. The Elk Code.
52. Laskowski R, Blaha P. Understanding the $L_{2,3}$ x-ray absorption spectra of early *3d* transition elements. *Phys Rev B*. 2010;82:205104.
53. Blaha P, Schwarz K, Tran F, Laskowski R, Madsen GKH, Marks LD. WIEN2k: An APW+lo program for calculating the properties of solids. *J Chem Phys*. 2020;152:Article 074101.
54. Tancogne-Dejean N, Oliveira MJT, Andrade X, Appel H, Borca CH, Le Breton G, Buchholz F, Castro A, Corni S, Correa AA, et al. Octopus, a computational framework for exploring light-driven phenomena and quantum dynamics in extended and finite systems. *J Chem Phys*. 2020;152:124119.
55. Tate J, Auguste T, Muller HG, Salières P, Agostini P, DiMauro LF. Scaling of wave-packet dynamics in an intense midinfrared field. *Phys Rev Lett*. 2007;98:Article 013901.
56. Shiner AD, Trallero-Herrero C, Kajumba N, Bandulet H-CC, Comtois D, Légaré F, Giguère M, Kieffer J-CC, Corkum PB, Villeneuve DM. Wavelength scaling of high harmonic generation efficiency. *Phys Rev Lett*. 2009;103:Article 073902.
57. Chen M-C, Mancuso C, Hernández-García C, Dollar F, Galloway B, Popmintchev D, Huang P-C, Walker B, Plaja L, Jaroń-Becker AA, et al. Generation of bright isolated attosecond soft X-ray pulses driven by multicycle midinfrared lasers. *Proc Natl Acad Sci USA*. 2014;111:E2361–E2367.
58. Buades B, Picón A, Berger E, León I, Di Palo N, Cousin SL, Cocchi C, Pellegrin E, Martin JH, Mañas-Valero S, et al. Attosecond state-resolved carrier motion in quantum materials probed by soft x-ray XANES. *Appl Phys Rev*. 2021;8:Article 011408.
59. Buades B, Picon A, Berger E, Leon I, Di Palo N, Cousin SL, Cocchi C, Pellegrin E, Martin JH, Mañas-Valero S, et al. Attosecond state-resolved carrier motion in quantum materials probed by soft X-ray XANES. arXiv. 2020. https://doi.org/10.1063/5.0020649
60. Jonas A, Stiel H, Glöggler L, Dahm D, Dammer K, Kanngießer B, Mantouvalou I. Towards Poisson noise limited optical pump soft X-ray probe NEXAFS spectroscopy using a laser-produced plasma source. *Opt Express*. 2019;27:36524–36537.
61. Kleine C, Ekimova M, Goldsztejn G, Raabe S, Strüber C, Ludwig J, Yarlagadda S, Eisebitt S, Vrakking MJJ, Elsaesser T, et al. Soft X-ray absorption spectroscopy of aqueous solutions using a table-top femtosecond soft X-ray source. *J Phys Chem Lett*. 2019;10:52–58.
62. Keitel B, Plönjes E, Kreis S, Kuhlmann M, Tiedtke K, Mey T, Schäferand B, Mann K. Hartmann wavefront sensors and their application at FLASH. *J Synchrotron Radiat*. 2016;23(1):43–49.
63. Wodzinski T, Künzel S, Koliyadu C, Jayanath P, Hussain M, Keitel B, Williams GO, Zeitoun P, Plönjes E, Fajardo M. High-harmonic generation wave front dependence on a driving infrared wave front. *Appl Opt*. 2020;1363–1370.
64. Chew A, Douguet N, Cariker C, Li J, Lindroth E, Ren X, Yin Y, Argenti L, Hill WT, Chang Z. Attosecond transient absorption spectrum of argon at the $L_{2,3}$ edge. *Phys Rev A*. 2018;97:Article 031407.
65. Giannozzi P, Baroni S, Bonini N, Calandra M, Car R, Cavazzoni C, Ceresoli D, Chiarotti GL, Cococcioni M, Dabo I, et al. QUANTUM ESPRESSO: A modular and open-source software project for quantum simulations of materials. *J Phys Condens Matter*. 2009;21:395502.
66. Pemmaraju CD. Simulation of attosecond transient soft x-ray absorption in solids using generalized Kohn–Sham real-time time-dependent density functional theory. *New J Phys*. 2020;22:Article 083063.
67. Novoselov KS, Mishchenko A, Carvalho A, Castro Neto AH. 2D materials and van der Waals heterostructures. *Science*. 2016;353(6298):aac9439.
68. Manzeli S, Ovchinnikov D, Pasquier D, Yazyev OV, Kis A. 2D transition metal dichalcogenides. *Nat Rev Mater*. 2017, 2017;2:Article 17033.
69. Ferrari AC, Bonaccorso F, Fal'ko V, Novoselov KS, Roche S, Bøggild P, Borini S, Koppens FHL, Palermo V, Pugno N, et al. Science and technology roadmap for graphene, related two-dimensional crystals, and hybrid systems. *Nanoscale*. 2015;7:4598–4810.
70. Lv R, Robinson JA, Schaak RE, Sun D, Sun Y, Mallouk TE, Terrones M. Transition metal dichalcogenides and beyond: Synthesis, properties, and applications of single- and few-layer Nanosheets. *Acc Chem Res*. 2015;48:56–64.
71. Sidiropoulos TPH, Di Palo N, Rivas DE, Severino S, Reduzzi M, Nandy B, Bauerhenne B, Krylow S, Vasileiadis T, Danz T, et al. Probing the energy conversion pathways between light, carriers, and lattice in real time with attosecond core-level spectroscopy. *Phys Rev X*. 2021;11:Article 041060.
72. Bunău O, Joly Y. Self-consistent aspects of x-ray absorption calculations. *J Phys Condens Matter*. 2009;21:345501.
73. Nagy T, Hädrich S, Simon P, Blumenstein A, Walther N, Klas R, Buldt J, Stark H, Breitkopf S, Jójárt P, et al. Generation of three-cycle multi-millijoule laser pulses at 318 W average power. *Optica*. 2019;6:1423–1424.
74. Eidam T, Hanf S, Seise E, Andersen TV, Gabler T, Wirth C, Schreiber T, Limpert J, Tünnermann A. Femtosecond fiber CPA system emitting 830 W average output power. *Opt Lett*. 2010;35:94–96.

75. Hrisafov S, Pupeikis J, Chevreuil P-A, Brunner F, Phillips CR, Gallmann L, Keller U. High-power few-cycle near-infrared OPCPA for soft X-ray generation at 100 kHz. *Opt Express*. 2020;28:40145–40154.
76. Kleine C, Ekimova M, Winghart M-O, Eckert S, Reichel O, Löchel H, Probst J, Braig C, Seifert C, Erko A, et al. Highly efficient soft x-ray spectrometer for transient absorption spectroscopy with broadband table-top high harmonic sources. *Struct Dyn*. 2021;8:Article 034302.
77. Bruner BD, Krüger M, Pedatzur O, Orenstein G, Azoury D, Dudovich N. Robust enhancement of high harmonic generation via attosecond control of ionization. *Opt Express*. 2018;26:9310–9322.
78. Martínez Vázquez R, Ciriolo AG, Crippa G, Tosa V, Sala F, Devetta M, Vozzi C, Stagira S, Osellame R. Femtosecond laser micromachining of integrated glass devices for high-order harmonic generation. *Int J Appl Glas Sci*. 2022;13:162–170.
79. Pacilé D, Papagno M, Rodríguez AF, Grioni M, Papagno L, Girit ÇÖ, Meyer JC, Begtrup GE, Zettl A. Near-edge X-ray absorption fine-structure investigation of graphene. *Phys Rev Lett*. 2008;101:Article 066806.